Collectivity of plasmonic excitations in small sodium clusters with ring and linear structures

doi: 10.1103/PhysRevA.83.013201

Collectivity of plasmonic excitations in small sodium clusters with ring and linear structures

Tomokazu Yasuike,[1] Katsuyuki Nobusada,[1,*] and Michitoshi Hayashi[2]

[1]*Institute for Molecular Science and The Graduate University for Advanced Studies (SOKENDAI), Myodaiji, Okazaki, Aichi 444-8585, Japan*

[2]*Center for Condensed Matter Sciences, National Taiwan University, Taipei 106, Taiwan, Republic of China*

(Received 5 October 2010; published 31 January 2011)

The collectivity of the electronic motion in finite systems is studied by using both the linear response density functional theory (LRDFT) and the collectivity index defined by the transition density matrix. We demonstrate a collectivity analysis on the size-dependent peaks of electronic excitations of small sodium clusters (rings and linear chains). We find the excitation-mode dependence of the collectivity and large collectivities for the higher-energy plasmonic excitations. The collectivity analysis also clarifies the existence of the nondipolar collective motion at the energies very close to the higher-energy plasmonic excitations. The importance of the nondipolar motion is pointed out in light of nano-optics.

DOI: 10.1103/PhysRevA.83.013201 PACS number(s): 36.40.Gk, 36.40.Vz, 73.21.−b

I. INTRODUCTION

Plasmonic excitations in metal nanoparticles have received much attention in the past few decades [1,2] because they play important roles in single molecular spectroscopy [3,4], catalytic reactions [5], biomedical treatments [6], and plasmonics [7]. They are associated with the collective electronic motion in classical mechanics, called plasma oscillations, and have been intensively studied by using the classical Maxwell equation for continuous bodies with parameters of geometrical shapes and dielectric constants [8–10]. Useful approximate methods for solving the Maxwell equation have been recently developed for particles with arbitrary shapes in complex environments [11–14], and the effects of size, shape, and dielectric environment on optical properties of metal nanoparticles were studied [15]. The field enhancement near metal nanoparticles found by these classical methods has been regarded as an important mechanism of the intensity enhancement for the surface-enhanced Raman scattering (SERS) in metal nanoparticles with nanogaps. However, the classical treatment is not necessarily suitable for discussing plasmonic excitations of metal nanoparticles in recent diverse applications. The quantum treatment is required for fully understanding properties of nanofabricated materials consisting of tens to hundreds of atoms, and the explicit description of individual electrons is indispensable when the hybridization in the wave functions of nanoparticles and their environments becomes important. Such a situation appears in single molecular spectroscopy and catalytic reactions because the electron transfer is essential in the processes involved [3–5]. Recently, Zuloaga, Prodan, and Nordlander showed [16] that the quantum treatment is required to estimate the field enhancement for narrow-gap nanoparticle dimers.

Quantum-mechanical studies of photoexcitation of metal clusters have also been carried out over many decades [17–24]. Although early interests were mainly in the size- and geometry-dependence of the photoabsorption spectra, several authors have discussed the collectivity of the plasmonic excitations in those spectra. Yannouleas, Broglia, and their coworkers [18–21] have reported an important series of studies about the collective excitations in alkali-metal clusters. They found that the transition moments of individual particle-hole–hole-particle excitations in spherical clusters were concentrated to essentially a single excited state and the corresponding excitation was assigned to a plasmonic excitation. In deformed clusters [21], the single plasmonic excitation splits into a plural of excitations due to their low symmetries. However, these excitations were also shown to be highly collective as the result of the transition-moment concentration and they were assigned to the plasmonic excitations. In the context of nanofabricated plasmonic materials, Yan and Gao [22,23] studied the plasmonic excitation of linear sodium clusters with time-dependent density functional theory (TDDFT). The chain-length dependence of the plasmonic excitations were systematically investigated and it was shown that the transition moments for these excitations were accumulated atom by atom with increasing number of atoms in the cluster. It manifests another type of concentration of transition moments different from the findings of Yannouleas and Broglia. These quantum-mechanical treatments clearly revealed the fact that metal nanoparticles acquire special sensitivities in interacting with light by the concentration of the transition moments. However, the mechanism behind this has not yet been sufficiently clarified. Recently, the large transition moments of the plasmonic excitations have been found to play an important role in the signal enhancement of SERS [25], and the mechanism for generating large transition moments has been an issue of great interest.

In the present article, we investigate the concentration mechanism of transition moment in the plasmonic excitations in small sodium clusters. To this end, we analyze the spatial distributions of transition densities and the collectivity of the plasmonic excitations by using the index derived from the transition density matrix. We also discuss the excitation-mode dependence of the collectivity and two mechanisms for the acquisition of large transition moments in sodium clusters. Finally, the nondipolar collective excitations are discussed in light of nano-optics.

*nobusada@ims.ac.jp

II. METHODS

A. Photoexcitation spectrum by linear-response density functional theory

Photoexcitation spectra are calculated by the conventional approach based on linear-response density functional theory (LRDFT) [26]. We make a brief review of the method of calculations. The electron density and the total energy of the ground state are obtained in terms of the Kohn-Sham (KS) orbitals $\{\phi_i(\boldsymbol{r})\}$ and their energies $\{\epsilon_i\}$ are determined by the KS equation [27]

$$\left(\frac{1}{2}\nabla^2 + v(\boldsymbol{r}) + \int \frac{\rho(\boldsymbol{r}')}{|\boldsymbol{r}-\boldsymbol{r}'|}d\boldsymbol{r}' + v_{\mathrm{XC}}(\boldsymbol{r})\right)\phi_i(\boldsymbol{r}) = \epsilon_i\phi_i(\boldsymbol{r}), \tag{1}$$

where $v(\boldsymbol{r})$, $\rho(\boldsymbol{r})$, and $v_{\mathrm{XC}}(\boldsymbol{r})$ are the nuclear attraction potential, electron density, and exchange-correlation functional, respectively. The linear response of the obtained ground state is determined by the eigenvalue problem

$$\begin{pmatrix} \mathbf{A} & \mathbf{B} \\ -\mathbf{B}^* & -\mathbf{A}^* \end{pmatrix}\begin{pmatrix} \mathbf{X}^n \\ \mathbf{Y}^n \end{pmatrix} = \omega_n \begin{pmatrix} \mathbf{X}^n \\ \mathbf{Y}^n \end{pmatrix}, \tag{2}$$

where vectors $\mathbf{X}^n$ and $\mathbf{Y}^n$ are formed by collecting the amplitudes for particle-hole (p-h) and hole-particle (h-p) pair excitations, respectively, in the KS orbital representation. The matrix elements of $\mathbf{A}$ and $\mathbf{B}$ are

$$A_{ia,jb} = (\epsilon_a - \epsilon_i)\delta_{ij}\delta_{ab} + 2K_{ia,jb}, \tag{3}$$

$$B_{ia,jb} = 2K_{ia,jb}, \tag{4}$$

where

$$K_{ia,jb} = \int d\mathbf{r}d\mathbf{r}'\phi_i^*(\mathbf{r})\phi_a(\mathbf{r})\left[\frac{1}{|\mathbf{r}-\mathbf{r}'|} + \frac{\delta v_{\mathrm{XC}}(\rho)}{\delta\rho}\delta(\mathbf{r}-\mathbf{r}')\right] \times \phi_b^*(\mathbf{r}')\phi_j(\mathbf{r}'). \tag{5}$$

Here, the indices i,j and a,b denote occupied (hole) and vacant (particle) orbitals, respectively. Since the working equation given by Eq. (2) is a non-Hermitian eigenvalue problem, the orthonormality relation is different from that for a Hermitian problem. Then, the relation is defined by

$$\sum_{ia}\left(X_{ia}^n X_{ia}^m - Y_{ia}^n Y_{ia}^m\right) = \delta_{n,m}. \tag{6}$$

The electric transition dipole moment μ_{0n} of the excitation from $|\Psi_0\rangle$ to $|\Psi_n\rangle$ is obtained by

$$\mu_{0n} = \langle\Psi_0|\hat{\mu}|\Psi_n\rangle = \sum_{ia}\sqrt{2}\left(X_{ia}^n\mu_{ia} + Y_{ia}^n\mu_{ia}^*\right), \tag{7}$$

where $\hat{\mu} \equiv -\mathbf{r}$ and $\mu_{ia} \equiv \int \phi_i^*(\mathbf{r})\hat{\mu}\phi_a(\mathbf{r})d\mathbf{r}$. The quantity μ_{ia} is the transition dipole moment for the individual excitation of $\phi_i \rightarrow \phi_a$. If the $\mathbf{B}$ matrix can be neglected, the eigenvalue problem is reduced to the form of $\mathbf{A}\mathbf{X}^n = \omega_n\mathbf{X}^n$ under the Tamm-Dancoff approximation (TDA). For the TDA, the orthonormality relationship and the transition dipole moment are given by setting $Y_{ia} = 0$ for all ia pairs in Eqs. (6) and (7).

B. Transition density

In the present work, we characterize the computed excitations by analyzing the transition density for the excitation $|\Psi_0\rangle \rightarrow |\Psi_n\rangle$. The transition density is defined by

$$\rho_{\mathrm{tr}}^{0n}(\mathbf{r}) = \langle\Psi_0|\sum_i^N \delta(\mathbf{r}-\mathbf{r}_i)|\Psi_n\rangle. \tag{8}$$

This quantity is related to a Fourier component of the time-dependent density distribution $\rho(\mathbf{r},t)$, as shown below. Under a weak perturbation, the electronic eigenstate becomes a wave packet and its time evolution is written as

$$|\Psi(t)\rangle = |\Psi_0\rangle + \sum_n c_n|\Psi_n\rangle e^{-i(E_n-E_0)t/\hbar}. \tag{9}$$

The corresponding time evolution of electronic density distribution is

$$\begin{aligned}\rho(\mathbf{r},t) &= \langle\Psi(t)|\sum_i^N \delta(\mathbf{r}-\mathbf{r}_i)|\Psi(t)\rangle \\ &= \rho_0(\mathbf{r}) + \sum_n c_n\rho_{\mathrm{tr}}^{0n}(\mathbf{r})e^{-i(E_n-E_0)t/\hbar} + \mathrm{c.c.},\end{aligned} \tag{10}$$

where $\rho_0(\mathbf{r}) = \langle\Psi_0|\sum_i^N \delta(\mathbf{r}-\mathbf{r}_i)|\Psi_0\rangle$ is the ground-state density. It follows that the transition density $\rho_{\mathrm{tr}}^{0n}(\mathbf{r})$ is proportional to the Fourier component of the time-dependent electronic density $\rho(\mathbf{r},t)$ at the frequency of $(E_n - E_0)/\hbar$. Therefore, we can grasp spatial information of the electronic motion during the excitation by inspecting the transition density, whereas the coefficient c_n depends on an explicit form of the perturbation. The transition density has dynamical information and is often more useful than the static electronic density difference given by

$$\delta\rho(\mathbf{r}) \equiv \langle\Psi_n|\sum_i^N \delta(\mathbf{r}-\mathbf{r}_i)|\Psi_n\rangle - \langle\Psi_0|\sum_i^N \delta(\mathbf{r}-\mathbf{r}_i)|\Psi_0\rangle. \tag{11}$$

Within the LRDFT, the transition density is written as

$$\rho_{\mathrm{tr}}^{0n}(\mathbf{r}) = \sum_{ia}\sqrt{2}\left[X_{ia}^n\phi_i^*(\mathbf{r})\phi_a(\mathbf{r}) + Y_{ia}^n\phi_a^*(\mathbf{r})\phi_i(\mathbf{r})\right]. \tag{12}$$

The integration of the transition density $\rho_{\mathrm{tr}}^{0n}(\mathbf{r})$ with the operator $\hat{\mu}$ gives μ_{0n}, as shown in Eq. (7).

C. Singular value decomposition analysis of transition density matrix

In the TDA, the off-diagonal rectangular block of the one-electron transition density matrix $\mathbf{T}$ is formed from p-h excitation amplitudes X_{ia} as $T_{i,a} = X_{ia}$. By using the method of the singular value decomposition (SVD), $\mathbf{T}$ is simplified to a generalized diagonal form [28] of

$$\mathbf{\Lambda} = \mathbf{U}^T\mathbf{T}\mathbf{V} = \begin{pmatrix} \lambda_1 & 0 & \ldots & 0 & 0 & \\ 0 & \lambda_2 & \ldots & 0 & 0 & \\ & & \ldots & & & \mathbf{0} \\ 0 & 0 & \ldots & \lambda_{n-1} & 0 & \\ 0 & 0 & \ldots & 0 & \lambda_n & \end{pmatrix}, \tag{13}$$

where the matrices **U** and **V** are determined from the following eigenvalue problems:

$$\mathbf{T}\mathbf{T}^{\dagger}\mathbf{U} = \mathbf{U}\boldsymbol{\eta}, \tag{14}$$

$$\mathbf{T}^{\dagger}\mathbf{T}\mathbf{V} = \mathbf{V}\boldsymbol{\eta}'. \tag{15}$$

Since SVD gives the transformation to the natural orbital representation [29], the vector $\boldsymbol{\lambda}$ defined by collecting the diagonal elements of $\boldsymbol{\Lambda}$ is the minimal representation of the excitation operator for an excited state. The excitation vector $\boldsymbol{\lambda}$ satisfies the following normalization condition:

$$\sum_{i=1}^{n_{\rm occ}} \lambda_i^2 = 1. \tag{16}$$

While it is mathematically proven that the maximum number of the nonzero elements is equal to the number of the occupied orbitals, only a few dominant excitations are known to usually contribute to each excited state in usual molecular systems [30]. In contrast, many excitations are expected to contribute to plasmonic excitation. To study the collectivity in electronic excitations, we use the notion of the inverse participation ratio (IPR) ν^*:

$$\nu^* = \frac{1}{\sum_{i=1}^{n_{\rm occ}} \lambda_i^4}, \tag{17}$$

which represents the effective number of excitations that contribute to the excitation vector. For instance, $\nu^* = 1$ when only one p-h pair contributes to the excitation, while $\nu^* = n_{\rm occ}$ when all excitation pairs equivalently contribute ($\lambda_i = 1/\sqrt{n_{\rm occ}}$). This notion has so far been used in many research fields [31–35]. For analysis of the configuration-interaction singles (CIS) wave functions, Luzanov first employed IPR to discuss the collectivity in electronic excitations [36].

For LRDFT, the transition density matrix cannot be straightforwardly defined owing to the unusual orthonormalization condition of Eq. (6). Luzanov and Zhikol [37] recently circumvented this difficulty by transforming the non-Hermitian eigenvalue problem to the Hermitian one. However, the transformation employed mixed the p-h and h-p spaces, and the relationship to the TDA was not necessarily clear. We alternatively define the pseudo transition density matrices as

$$T^X_{i,a} = \frac{X_{ia}}{\sqrt{\sum_{ia} X_{ia}^2}}, \quad T^Y_{i,a} = \frac{Y_{ia}}{\sqrt{\sum_{ia} Y_{ia}^2}}, \tag{18}$$

for p-h and h-p spaces, respectively. The above procedure for estimating the IPR is simply applicable to these matrices, and the IPRs (ν^*_X and ν^*_Y) are separately obtained for p-h and h-p spaces, respectively. The overall collectivity index n^* is calculated by averaging over these IPRs:

$$n^* = (\nu^*_X)^{\sqrt{\sum_{ia} X_{ia}^2}} (\nu^*_Y)^{\sqrt{\sum_{ia} Y_{ia}^2}}. \tag{19}$$

D. Computational details

To investigate the size- and geometry-dependence of plasmonic excitations, we studied the photoexcitation of the Na_n ($n = 6$, 10, and 14) clusters with the ring and linear geometries. The lengths for all the bonds in the clusters are assumed to be 3.72 Å, being the free-dimer bond length and the same value as employed by Yan and Gao [23]. Although these geometries are not necessarily local minima of the clusters in the vacuum, we employed these structures as prototypes for studying general aspects of plasmonic excitation without discussing the detailed electronic structures of the systems. Moreover, recent advanced experimental techniques to manipulate adsorbate atoms on solid surfaces enable us to locate sodium atoms in arbitrary topological arrangements, and thus our numerical experiment can, in principle, be realized.

The sodium atom is described by the norm-conserving pseudopotential [38], and only the 3s electron is explicitly included in the calculations. Three-dimensional uniform grids are used for the spatial representation, and the local-density approximation (LDA) [39] is employed for $v_{\rm XC}$.

III. RESULTS AND DISCUSSION

A. Electronic motion characterizing plasmonic excitation

Figure 1 shows the photoabsorption spectra for the ring Na_6, Na_{10}, and Na_{14} clusters. Each peak was broadened using a Gaussian distribution function with full width at half maximum of $0.1\sqrt{4\ln 2/\pi}$ eV (∼0.094 eV). By setting this value, the peak intensity becomes equal to ten times the transition moment for each peak. For low-lying excitations, the dimension of the p-h (h-p) excitation space can be largely reduced without affecting the computational accuracy. The dimensions employed were 81, 125, and 168 for Na_6, Na_{10},

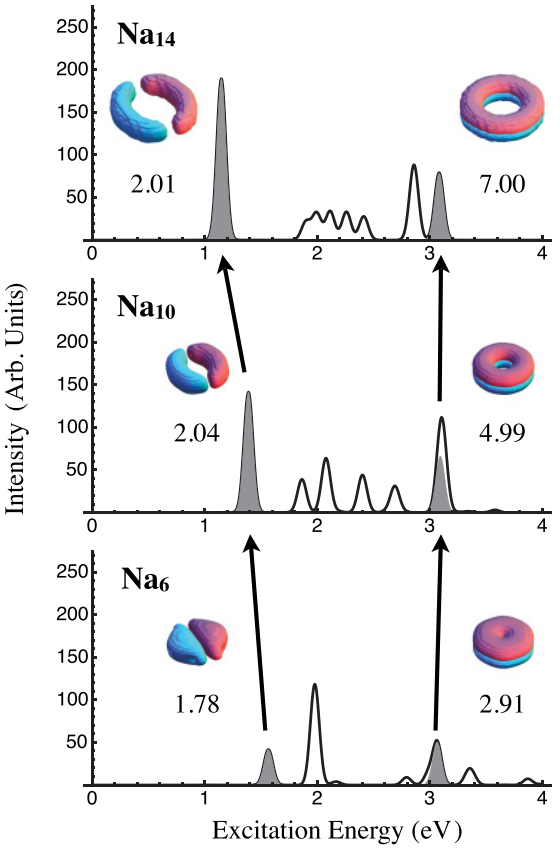

FIG. 1. (Color online) Photoabsorption spectra for ring Na_n clusters ($n = 6$, 10, and 14). The color insets illustrate the transition density distributions for plasmonic excitations.

and Na_{14}, respectively. In each excitation space, there are 41, 65, and 83 dipole-allowed excitations for Na_6, Na_{10}, and Na_{14}, respectively. However, the photoabsorption spectra clearly show that only a small number of strong peaks appear. Although this fact seems to imply the concentration of the transition moments, it will be shown in Sec. III B that such a speculation is not always correct. The color insets in Fig. 1 illustrate the transition-density distributions for some representative excitations indicated by the gray-shaded areas. The red and blue colors denote the increase and decrease, respectively, in the electron density that are different from that in the ground state. The transition-density distributions for the lower-energy excitations at 1.57 (Na_6), 1.39 (Na_{10}), and 1.15 eV (Na_{14}) show that these excitations cause the dipolar electronic motion in the weakly confined direction parallel to the ring plane. On the other hand, the dipolar motion along the strongly confined direction perpendicular to the ring plane is induced by the excitations at higher energies of 3.07, 3.09, and 3.08 eV for Na_6, Na_{10}, and Na_{14}, respectively. These are consistent with the intuition that the motion of more confined electrons requires large excitation energies. As indicated by the arrows in the figure, the transition moments for these excitations grow with increasing cluster size. They can be assigned to plasmonic excitations. This is another type of concentration of transition moments as was found by Yan and Gao [22,23]. Therefore, the two types of transition-moment concentrations mentioned in the introduction were actually observed for the Na ring clusters.

Figure 2 shows the photoabsorption spectra for the linear Na_6, Na_{10}, and Na_{14} clusters. The general features are qualitatively similar to those for the ring clusters. Only a small number of peaks have large transition moments, even though there are 40, 63, and 84 dipole-allowed excitations for Na_6, Na_{10}, and Na_{14}, respectively. The transition moments for the excitation inducing dipolar electronic motion grow with increasing cluster size and they are assigned to plasmonic excitations.

The simple dipolar picture of the motion generally becomes worse for small particles. In fact, the plasmonic excitations of the linear Na_6 cluster give transition densities more complicated than the simple dipolar distribution. However, the deviations from the dipolar distribution are immediately reduced for the linear Na_{10} cluster, and this implies that the electrons in the Na clusters have a strong tendency to collectively behave like a liquid droplet. Such a droplet picture has been known to be qualitatively valid for various types of nuclear matter [40].

B. Collectivity of electronic excitations and two mechanisms of large transition moments

Let us here quantitatively explain the collectivity of the plasmonic excitation by introducing the collectivity index n^* defined by Eq. (19). The indices for the plasmonic excitations are indicated in Figs. 1 and 2. We take here the case of Na_{10} and discuss the collectivity of the plasmonic excitations in detail. A similar discussion is valid for all the sizes of the clusters. The plasmonic excitations at the higher energies in both geometries have large values of n^*. The maximum value of n^* is five for Na_{10} because it has 10 valence electrons

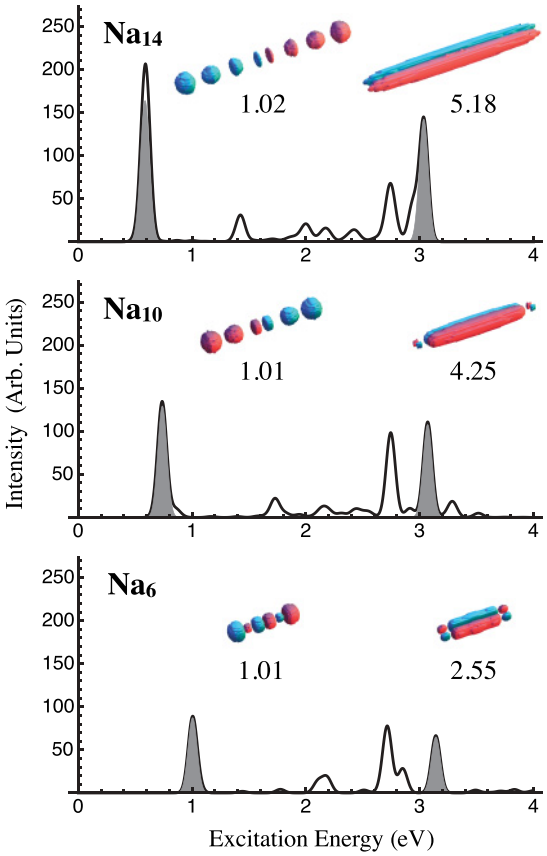

FIG. 2. (Color online) Same as Fig. 1 but for linear Na_n clusters ($n = 6$, 10, and 14).

and five occupied orbitals. Thus, the values of $n^* = 4.99$ (ring) and 4.25 (linear) mean that almost all the electron pairs contribute to the electronic motion induced by the plasmonic excitations at the higher energies. In contrast, the lower-energy plasmonic excitations give small values of n^*. In particular, the lower-energy plasmonic excitation of the linear Na_{10} cluster gives $n^* = 1.01$, and thus only one p-h (h-p) pair contributes to the excitation.

The origin of large transition moments is intuitively considered to be in the collectivity of electronic motion. However, the lower-energy plasmonic excitation of the linear Na_{10} cluster with the large transition moment has a small collectivity index. Therefore, we need to elucidate the mechanism that leads to large transition moments. To this end, we calculate the excitation spectrum by neglecting the interaction between the individual excitations in LRDFT [Fig. 3(a)] and compare it with the original LRDFT spectrum [Fig. 3(b)]. In Fig. 3(a), a strong individual excitation peak appears at 1.44 eV. The peak shifts toward lower energy (0.74 eV) when including the interaction between the individual excitations, whereas its transition moment is not redistributed to other peaks. The transition density for this individual excitation is shown in Fig. 4(a). This dipolar motion along the molecular axis of the linear cluster gives large transition moment because the charge-transfer distance is long. This is the reason for that the lower-energy plasmonic excitation has the large transition moment despite its low collectivity. In this sense, such a

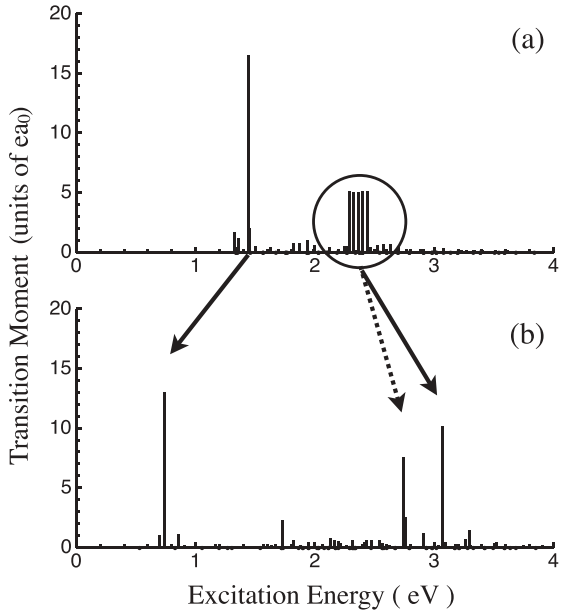

FIG. 3. Spectral change due to the configuration interaction between individual excitations: (a) Excitation spectrum of the linear Na_{10} cluster obtained by neglecting all the off-diagonal elements of **A** and **B** matrices. (b) LRDFT spectrum of the linear Na_{10} cluster. The vertical axis shows the transition dipole moment for each peak.

"plasmonic excitation" should be regarded as a long-range charge transfer excitation.

For the higher-energy plasmonic excitation, the reason for its large transition moment is completely different from that for the lower-energy one. We numerically confirmed by inspecting the eigenvector that the higher-energy plasmonic excitation mainly consists of five individual excitations at ~2.36 eV. The transition densities for these individual excitations are shown in Fig. 4(b). All the transition densities are delocalized over the whole spatial region of the cluster and show the dipolar electronic motion perpendicular to the molecular axis. Since all of them are related to the one-quantum excitation in the direction perpendicular to the molecular axis, the individual excitation energies are nearly degenerate. Moreover, it is easily understood from these transition densities that the interaction between these individual excitations are of the same order of magnitude. In fact, the TDA matrix **A** approximately has the simple structure of

$$\mathbf{A} \sim \begin{pmatrix} a & b & b & b & b \\ b & a & b & b & b \\ b & b & a & b & b \\ b & b & b & a & b \\ b & b & b & b & a \end{pmatrix}, \tag{20}$$

where the averaged values of a and b are 2.363 eV and 0.178 eV, respectively. From the structure of this matrix, the vector $(1,1,1,1,1)/\sqrt{5}$ is immediately found to be the eigenvector with the eigenvalue of $a + 4b$. The value of $a + 4b$ is 3.075 eV and is in good agreement with the actual excitation energy of 3.070 eV. For this state, the individual transition moments are constructively superposed by following Eq. (7), and the transition moment for the high-energy plasmonic excitation becomes approximately $\sqrt{5}$ times larger than the value for the individual excitation. The averaged value of the individual transition moment $\tilde{\mu}$ is 2.481 a.u. and then $\sqrt{5}\tilde{\mu}$ becomes 5.548 a.u. The LRDFT value is 5.383 a.u. and the agreement between them is semiquantitative. More quantitatively, the contributions from the two atoms on the edge of the cluster should be removed because they form the edge-localized mode, as found by Yan, Yuan, and Gao [22]. The analysis of the ring cluster was also made. We have confirmed that the relationship between the collectivity and the transition moment for the lower- and higher-energy plasmonic excitations is explained in the same way as in the linear cluster.

C. Existence of nondipolar collective motions

We have focused on the optically allowed excitations so far. However, the importance of nondipolar excitations has recently been recognized in the research field of nano-optics [41], and thus the existence of nondipolar collective excitations should be considered in the present plasmonic clusters. Figure 5 shows the transition densities for the excitations that have the four largest collectivity indices for the ring Na_{10} cluster. As clearly shown in this figure, these transition densities

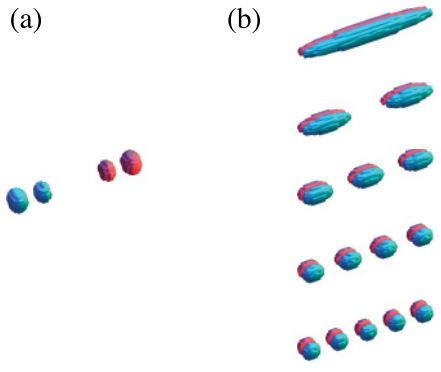

FIG. 4. (Color online) Transition densities for the individual excitations involved in the plasmonic excitations of the linear Na_{10} cluster: the plasmonic excitations at (a) 0.74 eV and (b) 3.07 eV.

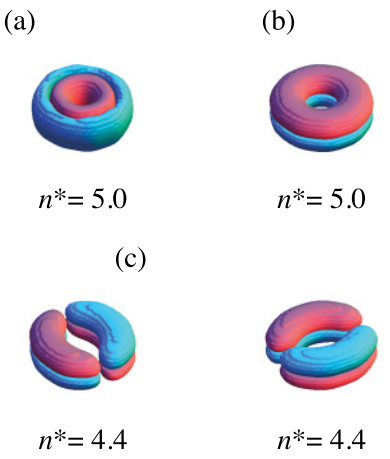

FIG. 5. (Color online) Transition densities for the excitations with n^* in the ring Na_{10} cluster: (a) monopole, (b) dipole, and (c) quadrupole excitations.

are delocalized over the whole spatial region of the cluster and correspond to the monopole, dipole, and quadrupole collective motions, respectively. It should be emphasized that these excitations are energetically near-degenerate to each other. The excitation energies are 3.09 (monopole), 3.16 (dipole), and 3.08 (quadrupole) eV. Therefore, not only the dipole mode but also the monopole and quadrupole modes are expected to play an important role in the resonant energy transfer between the ring clusters. Let us assume that two ring clusters are placed nearby. If the resonant light for the dipole plasmon mode is locally irradiated on the one of these two clusters, the dipolar electronic oscillation with the frequency corresponding to the excitation energy is induced in the cluster. By this local dipole oscillation, not only the dipole but also the other collective motions must be induced in the neighboring cluster. In particular, the above modes are collective and energetically near-degenerate, and the excitation transfer would effectively occur.

IV. CONCLUSION

We have quantified the plasmonic excitations in small sodium clusters in terms of collectivity index, which allows us to study the nature of collective motions of electrons in ring and linear-chain geometries. We found that sodium nanostructures generally have plasmonic excitations irrespective of their geometries. The transition density distribution clearly shows that the strong peaks are assigned to the dipolar collective motions. The dipolar motions have three directions, and the energies of the corresponding plasmonic excitations are degenerate for a spherical particle. In the present clusters, the plasmonic excitations split into higher- and lower-energy modes owing to their lower symmetries. The lower-energy mode is attributed to the electronic motion along the direction where the electrons can move through a longer distance. In this case, the clusters have large transition moments although the corresponding collectivity indices are small. Therefore, we regard the lower-energy mode, which was called L-mode plasmon by Yan, Yuan, and Gao [22], as a long-range charge transfer excitation. In contrast, the higher-energy plasmonic excitation is highly collective as a result of equal-strength interactions among energetically degenerate individual electronic states. In the vicinity of the higher-energy plasmonic excitation, we found that nondipolar collective modes exist. They are expected to play an important role in the interaction between nanoparticles in the context of nano-optics.

ACKNOWLEDGMENTS

This research was supported by Grant-in-Aid (No. 21350018) from the Ministry of Education, Culture, Sports, Science and Technology of Japan and by the Asian CORE program from Japan Society for the Promotion of Science. M.H. thanks Grants NSC(No. 99-2628-M-002-009-), NTU(No. 99R80827) and NCTS for their support.

[1] W. A. Murray and W. L. Barnes, Adv. Mater. **19**, 3771 (2007).
[2] U. Kreibig and M. Vollmer, *Optical Properties of Metal Clusters* (Springer, Berlin, 1995).
[3] S. Nie and S. R. Emory, Science **275**, 1102 (1997).
[4] H. Xu, E. J. Bjerneld, M. Käll, and L. Börjesson, Phys. Rev. Lett. **83**, 4357 (1999).
[5] A. T. Bell, Science **299**, 1688 (2003).
[6] L. R. Hirsch, R. J. Stafford, J. A. Bankson, S. R. Sershen, B. Rivera, R. E. Price, J. D. Hazle, N. J. Halas, and J. L. West, Proc. Natl. Acad. Sci. USA **100**, 13549 (2003).
[7] S. A. Maier and H. A. Atwater, J. Appl. Phys. **98**, 011101 (2005).
[8] G. Mie, Ann. Phys. **25**, 377 (1908).
[9] R. Gans, Ann. Phys. **47**, 270 (1915).
[10] S. Link, M. B. Mohanmed, and M. A. El-Sayed, J. Phys. Chem. B **103**, 3073 (1999).
[11] E. M. Purcell and C. R. Pennypacker, Astrophys. J. **186**, 705 (1973).
[12] B. T. Draine and P. J. Flatau, J. Opt. Soc. Am. A **11**, 1491 (1994).
[13] W. H. Yang, G. C. Schatz, and R. P. Van Duyne, J. Chem. Phys. **103**, 869 (1995).
[14] E. Moreno, D. Erni, C. Hafner, and R. Vahldieck, J. Opt. Soc. A **19**, 101 (2002).
[15] K. L. Kelly, E. Coronado, L. L. Zhao, and G. C. Schatz, J. Phys. Chem. B **107**, 668 (2003).
[16] J. Zuloaga, E. Prodan, and P. Nordlander, Nano Lett. **9**, 887 (2009).
[17] V. Bonačić-Koutecký, P. Fantucci, and J. Koutecký, Chem. Rev. **91**, 1035 (1991).
[18] C. Yannouleas, R. A. Broglia, M. Brack, and P. F. Bortignon, Phys. Rev. Lett. **63**, 255 (1989).
[19] C. Yannouleas and R. A. Broglia, Phys. Rev. A **44**, 5793 (1991).
[20] C. Yannouleas, E. Vigezzi, and R. A. Broglia, Phys. Rev. B **47**, 9849 (1993).
[21] M. Bernath, C. Yannouleas, and R. A. Broglia, Phys. Lett. A **156**, 307 (1991).
[22] J. Yan, Z. Yuan, and S. Gao, Phys. Rev. Lett. **98**, 216602 (2007).
[23] J. Yan and S. Gao, Phys. Rev. B **78**, 235413 (2008).
[24] K.-Y. Lian, P. Sałek, M. Jin, and D. Ding, J. Chem. Phys. **130**, 174701 (2009).
[25] L. Zhao, L. Jensen, and G. C. Schatz, J. Am. Chem. Soc. **128**, 2911 (2006).
[26] M. E. Casida, in *Recent Advances in Density Functional Methods*, Part I, edited by D. P. Chong (Singapore, World Scientific, 1995), p. 155.
[27] W. Kohn and L. J. Sham, Phys. Rev. **140**, 1133 (1965).
[28] I. Mayer, Chem. Phys. Lett. **437**, 284 (2007).
[29] P. R. Surján, Chem. Phys. Lett. **439**, 393 (2007).
[30] A. Dreuw and M. Head-Gordon, Chem. Rev. **105**, 4009 (2005).
[31] D. J. Thouless, Phys. Rep. **13**, 93 (1974).
[32] J. A. Leegwater, J. Phys. Chem. **100**, 144033 (1996).
[33] S. Mukamel, S. Tretiak, T. Wagersreiter, and V. Chernyak, Science **277**, 781 (1997).

[34] S. Tretiak and S. Mukamel, Chem. Rev. **102**, 3171 (2002).
[35] T. Yasuike and K. Someda, Phys. Rev. A **66**, 053410 (2002).
[36] A. V. Luzanov and V. E. Umanski, Theor. Exp. Chem. **13**, 162 (1977).
[37] A. V. Luzanov and O. A. Zhikol, Int. J. Quantum Chem. **110**, 902 (2010).
[38] N. Troullier and J. L. Martins, Phys. Rev. B **43**, 1993 (1991).
[39] J. P. Perdew and A. Zunger, Phys. Rev. B **23**, 5048 (1981).
[40] P. Ring and P. Schuck, *The Nuclear Many-Body Problem* (Springer-Verlag, Berlin Heidelberg, 1980).
[41] T. Iwasa and K. Nobusada, Phys. Rev. A **80**, 043409 (2009).